

A Whole-Body Disturbance Rejection Control Framework for Dynamic Motions in Legged Robots

Bolin Li¹, Wentao Zhang¹, Xuecong Huang¹, Lijun Zhu², and Han Ding³

Abstract—This letter presents a control framework for legged robots that enables self-perception and resistance to external disturbances and model uncertainties. First, a novel disturbance estimator is proposed, integrating adaptive control and extended state observers (ESO) to estimate external disturbances and model uncertainties. This estimator is embedded within the whole-body control framework to compensate for disturbances in the legged system. Second, a comprehensive whole-body disturbance rejection control framework (WB-DRC) is introduced, accounting for the robot's full-body dynamics. Compared to previous whole-body control frameworks, WB-DRC effectively handles external disturbances and model uncertainties, with the potential to adapt to complex terrain. Third, simulations of both biped and quadruped robots are conducted in the Gazebo simulator to demonstrate the effectiveness and versatility of WB-DRC. Finally, extensive experimental trials on the quadruped robot validate the robustness and stability of the robot system using WB-DRC under various disturbance conditions.

Index Terms—Legged robots, humanoid and bipedal locomotion, whole-body motion planning and control, disturbance rejection control.

I. INTRODUCTION

LEGGED robots have gained significant attention in recent years due to their ability to navigate complex and uneven terrain [1], offering substantial advantages in a wide range of applications, such as search and rescue, exploration, and assistive robotics. However, one of the main challenges in legged robot locomotion is the ability to maintain stability and robustness in the face of external disturbances and model

Received 17 June 2025; accepted 5 July 2025. Date of publication; date of current version. This article was recommended for publication by Associate Editor K.Akbari Hamed and Editor A.Kheddar upon evaluation of the reviewers' comments. This work was supported in part by the National Natural Science Foundation of China under Grant 62173155 and Grant 52188102 and in part by the Taihu Lake Innovation Fund for Future Technology, HUST. (Corresponding author: Lijun Zhu)

¹Bolin Li, Wentao Zhang, and Xuecong Huang are with the School of Artificial Intelligence and Automation, Huazhong University of Science and Technology, Wuhan 430074, China bolin_li@hust.edu.cn, wentaozhang@hust.edu.cn, M20237351@hust.edu.cn

²Lijun Zhu is with the School of Artificial Intelligence and Automation, Huazhong University of Science and Technology, Wuhan 430074, China, and also with the State Key Laboratory of Intelligent Manufacturing Equipment and Technology, Huazhong University of Science and Technology, Wuhan 430074, China ljzhu@hust.edu.cn

³Han Ding is with the State Key Laboratory of Intelligent Manufacturing Equipment and Technology, Huazhong University of Science and Technology, Wuhan 430074, China, and also with the School of Mechanical Science and Engineering, and the State Key Laboratory of Intelligent Manufacturing Equipment and Technology, Huazhong University of Science and Technology, Wuhan 430074, China dinghan@hust.edu.cn

This article has supplementary downloadable material available at <https://doi.org/10.1109/LRA.2025.3588716>, provided by the authors.

Digital Object Identifier 10.1109/LRA.2025.3588716

uncertainty, such as ground irregularities, unexpected external forces, heavy loads, or changes in terrain conditions. These disturbances can significantly affect the robot's state and lead to deviations from the desired trajectory, ultimately compromising the performance and stability.

To enhance the robustness of legged robots, various methods for disturbance rejection have been developed and implemented. One approach involves the design of sophisticated controllers, such as limit cycle walkers [2], [3] and high-performance optimal control [4], [5], to improve disturbance rejection. The article [5] presents a novel adaptive control methodology integrated into a force-based control system, enabling agile-legged robots to carry heavy loads while maintaining dynamic motion over rough terrain, as demonstrated experimentally on the Unitree A1 robot. Another approach utilizes disturbance rejection observers [6] to further enhance the robot's robustness. The general momentum observer is a useful method for the disturbance perception. Initially developed for collision detection and disturbance perception in robotic manipulator arm systems [7], this approach has been widely adopted in recent years for legged systems [6], [8], [9]. In [6], a proprioceptive-based disturbance estimator is proposed, which effectively filters foot-ground interaction noise and suppresses estimation errors. It is paired with a hierarchical whole-body controller that accounts for full-body dynamics, actuation limits, external disturbances, and interactive constraints. In [8], a discrete-time extension of the generalized-momentum disturbance observer is presented to enhance the accuracy of proprioceptive force control estimates, with the information fused with other contact priors under a Kalman filtering framework to improve the robustness of the method. In [9], an external disturbance estimator was proposed for legged robots based on the system's momentum, integrating a motion planner, an optimization problem for ground reaction forces, and a whole-body controller, which is tested on a quadruped robot in a dynamic simulation. These generalized-momentum disturbance observer rely on the assumption that the relationship between the inertia matrix and the Coriolis matrix of the Euler-Lagrange system holds, as discussed in [8], which limits their applicability. Although disturbance observers are effective for external disturbance rejection and compensation in legged robots, they encounter difficulties in handling model uncertainties and fault tolerance, especially in robots with complex dynamic interactions and inaccurate motor output torque. Previous model-based control methods for addressing uncertainties in legged robots either overlooked high-level planning and model uncertainties [6],

failed to account for external disturbances and fault tolerance [4], [10], or failed to incorporate fault tolerance and achieve performance based on a simplified rigid body model [5]. Additionally, these approaches in [4], [5], [10] were based on single rigid-body dynamics and primarily applied to quadruped robots, making them less suitable for bipedal and humanoid robots.

An active disturbance rejection control strategy (ADRC) was developed in [11] to address plants with significant uncertainties in both dynamics and external disturbances [12], [13]. The core design of ADRC involves using an ESO to estimate generalized disturbances and compensate for them in a feedforward manner. Subsequently, a simple proportional-derivative control law is synthesized to ensure bounded-error tracking performance. While ADRC is effective in handling various modeling uncertainties when they are accurately estimated by the ESO, it does not explicitly account for parameterizable uncertainties, which increases the learning burden on the ESO. As a result, compared to adaptive control, ADRC tends to exhibit poorer tracking performance in systems with substantial parametric uncertainties [14]. The adaptive control approach is typically used to address parametric uncertainties within a single controller [5], [10]. By integrating adaptive control and ESO through the full-state feedback, where parametric uncertainties and uncertain nonlinearities are handled separately, improved tracking performance can be achieved, as verified in hydraulic servo systems [14].

Unlike previous work, we develop a novel disturbance estimator that addresses model uncertainty, external disturbances, and fault tolerance, integrating it into the control architecture of legged robots. Our approach combines the ESO and adaptive control to estimate disturbances while considering whole-body uncertainties. Inspired by the work in [5], we adopt a new form for model uncertainty, incorporating unknown parameters and nonlinearities, rather than estimating a total disturbance. This form offers better physical interpretability and enhances disturbance rejection performance. The main contributions and important emphases are the following:

1) A novel disturbance estimator has been introduced, integrating adaptive control and an ESO to estimate uncertainties in the legged system. The stability and boundedness of the proposed estimator are guaranteed with or without uncertainties.

2) A general whole-body disturbance rejection control framework is proposed and is integrated into a hierarchical control architecture of legged robots.

3) Simulations are conducted on both biped and quadruped robots, and experiments are carried out on the Unitree A1 quadruped robot to verify the effectiveness of the proposed WB-DRC, as well as its advantages in terms of robustness and stability.

This letter is organized as follows. Section II provides the background on legged robots. Section III presents the high-level control. Section IV introduces the adaptive extended state disturbance rejection estimator. Section V presents the whole-body disturbance rejection planner. Sections VI and VII evaluate the performance of the proposed framework through simulation and on a physical prototype, respectively. Finally,

Section VIII concludes the letter.

II. PRELIMINARIES

The whole-body dynamics of a floating-base robot can be written as

$$D(q)\ddot{q} + C(\dot{q}, q)\dot{q} + G(q) = S^\top \tau + J(q)^\top F + d \quad (1)$$

where $q := [(q^b)^\top, (q^j)^\top]^\top \in \mathbb{R}^{6+n}$ with $q^b \in \mathbb{R}^6$ being the pose of the floating base and q^j being the actuated joint positions. $d \in \mathbb{R}^{6+n}$ is the uncertainty, $D(q) \in \mathbb{R}^{(6+n) \times (6+n)}$ is a positive definite inertia matrix, $C(\dot{q}, q) \in \mathbb{R}^{(6+n) \times (6+n)}$ is the Coriolis matrix, $G(q) \in \mathbb{R}^{6+n}$ is the gravity vector; $S = [0_{n \times 6}, I_n]$ is the selection matrix of the actuation; $\tau \in \mathbb{R}^n$ is the actuation torques; $F \in \mathbb{R}^{3n_c}$ is the ground reaction forces (GRFs) of the stance leg; $J(q)^\top F \in \mathbb{R}^{(6+n) \times 3n_c}$ represents the ground reaction forces projected to the joints space, where $J(q)$ is the contact-dependent Jacobian matrix; n and n_c represent the number of active degrees of freedom and the number of legs in the support surface, respectively. For a humanoid robot with rectangular feet, the contact points correspond to the four vertices of the rectangular shape [15].

For the high-level planning, we will use centroidal dynamics that describes the change of the linear and angular momentum with respect to the external wrench. Denote by $c \in \mathbb{R}^3$ the position of the COM in the inertial frame, h the linear momentum and L the angular momentum around the COM of the robot. The linear momentum is $h = m\dot{c}$ with m being the total mass of the robot. The centroidal dynamics [16] can be obtained according to the Newton-Euler law as:

$$\begin{aligned} \dot{h} &= \sum_{i=1}^{n_c} f_i - mg \\ \dot{L} &= \sum_{i=1}^{n_c} (p_i - c) \times f_i \end{aligned} \quad (2)$$

where $f_i \in \mathbb{R}^3$ represents the ground reaction force of contact i , p_i denotes the position of contact i , and $g = [0 \ 0 \ 9.81]^\top$ is the gravity vector.

In this letter, we adopt the hierarchical control architecture used in [17]. As in Fig. 1, the robot's control system consists of several modules, including a high-level controller, low-level controller, state estimation, and gait scheduler. The user input module receives the robot's speed command from the user input, and the gait scheduler module determines the contact times and sequences with $s_m \in \{1 = \text{contact}, 0 = \text{swing}\}$. The high-level control module employs the model predictive control (MPC) based on the centroidal dynamics to generate reference trajectories for the system state and inputs of the whole-body dynamics, which are then provided to the low-level leg control module. The low-level control module receives the reference trajectories and implements the whole-body control (see [18]) or inverse dynamics to maintain the balanced locomotion.

To handle the unmodel dynamics and unknown external disturbance for the legged locomotion, a novel disturbance rejection whole-body control scheme is proposed and implemented in the low-level leg control module in this paper. The proposed scheme is shown in Fig. 2. We establish a disturbance

estimator based on the whole-body dynamics to estimate the system uncertainty, which is compensated by the whole-body planner.

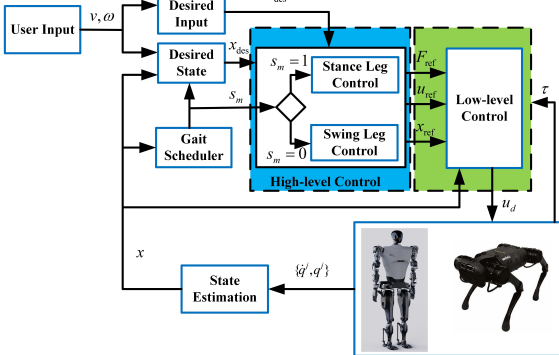


Fig. 1: Block diagram of a control architecture for legged robots.

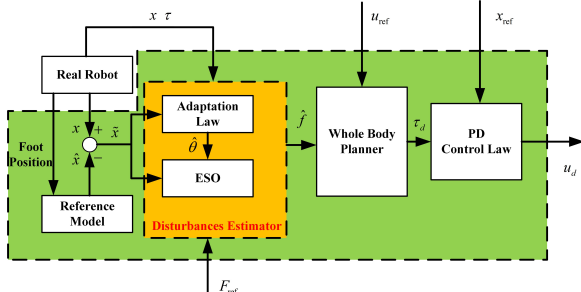


Fig. 2: Block diagram of the WB-DRC.

III. HIGH-LEVEL CONTROL

In this section, we use the centroidal dynamics (2) for the high-level planning via the MPC. Denote $x_c = [h^\top, L^\top, q^\top]^\top$, $u_c = [F_c^\top, (\dot{q}^j)^\top]^\top$ with $F_c = [f_1^\top, \dots, f_{n_c}^\top]^\top \in \mathbb{R}^{3n_c}$. The centroidal dynamics (2) can be rewritten as

$$\dot{x}_c = f_c(x_c, u_c) \quad (3)$$

where $f_c(x_c, u_c)$ can be deduced from (2). The linear and angular momentum are related to the joint velocity via the centroidal command matrix $A(q)$ [19]

$$\begin{bmatrix} h \\ L \end{bmatrix} = A(q)\dot{q}. \quad (4)$$

The continuous dynamics (3) is discretized over intervals of the prediction horizon $[t, t+T]$ for the nonlinear trajectory optimization problem. We consider the total number of steps in the MPC to be N , and thus the duration of each discrete interval is $\delta t = T/(N-1)$. Define $J_c(x)$ as the terminal quadratic cost around the reference state x_{des} :

$$J_c(x) = (x - x_{\text{des}}(T))^\top Q_t(x - x_{\text{des}}(T))$$

and $\varphi_c(x, u)$ as the quadratic cost around the reference state x_{des} and input u_{des} :

$$\begin{aligned} \varphi_c(x, u) &= (x - x_{\text{des}}(T))^\top Q_s(x - x_{\text{des}}(T)) \\ &+ (u - u_{\text{des}}(T))^\top R(u - u_{\text{des}}(T)). \end{aligned}$$

Let $x_{i,k}$ and $u_{i,k}$ denote the sequences of state and input variables in the MPC at the k -th solve, respectively, for $i = 1, \dots, N$. The nonlinear MPC problem can be formulated by defining and evaluating a cost function and constraints on the grid of nodes as

$$\begin{aligned} \min_{X, U} \quad & J_c(x_{N,k}) + \sum_{k=0}^{N-1} \varphi_{c,i}(x_{i,k}, u_{i,k}) + l_i(x_{i,k}, u_{i,k}) \\ \text{s.t.} \quad & x_{0,k} - x_{m,k} = 0, \\ & x_{i+1,k} - x_{i,k} - f_c(x_{i,k}, u_{i,k})\delta t = 0, \\ & g_i(x_{i,k}, u_{i,k}) = 0, \quad i = 0, \dots, N-1. \end{aligned} \quad (5)$$

where $x_{m,k}$ is the current measured state, $X = [x_{0,k}^\top, \dots, x_{N,k}^\top]^\top$ and $U = [u_{0,k}^\top, \dots, u_{N-1,k}^\top]^\top$ are the sequences of state and input variables respectively. The process of establishing these constraints l_i and g_i follows the same approach as described in [18]. The penalized cost function l_i is derived from inequality constraints, which describe the requirement that the swing leg remains above the ground and the contact force lies within the friction cone. The constraint function g_i captures the equality requirements that the swing leg's end does not experience a contact force, and that the end of the stance leg has zero velocity. Note that the legged robot is a hybrid system, where the GRFs are either zero or non-zero, as determined by the constraint g_i , which is managed by the gait scheduler module.

In centroidal dynamics (2), referred to as nominal centroidal dynamics, the force f_i is considered the ground reaction force without accounting for external forces, and m is treated as the robot's nominal mass, excluding model uncertainties. We use the nominal centroidal dynamics instead of its disturbed version, which incorporates external forces and model uncertainties, because we aim to generate the reference trajectory as if the system is unaffected by disturbances. The low-level control will compensate the the disturbance in the whole-body dynamics (1) and intends to track the reference trajectory generated from the nominal system.

The solution to the MPC problem (5) is denoted as $X = X_{\text{ref}} := [h_{\text{ref}}^\top, L_{\text{ref}}^\top, q_{\text{ref}}^\top]^\top$ and $U = U_{\text{ref}} := [F_{\text{ref}}^\top, (\dot{q}_{\text{ref}}^j)^\top]^\top$, which gives the reference signals at the discrete time instances $[t, t+\delta t, \dots, t+T]^\top$. We can linearly interpolate the discrete reference signals to a continuous reference trajectory for the interval $[t, t+T]$. The reference velocity is given by

$$\dot{q}_{\text{ref}}^b = \begin{bmatrix} \dot{q}_{\text{ref}}^b \\ \dot{q}_{\text{ref}}^j \end{bmatrix}. \quad (6)$$

The reference velocity \dot{q}_{ref}^b for the base can be obtained as

$$\dot{q}_{\text{ref}}^b = A_b^{-1}(q_{\text{ref}}) \left(\begin{bmatrix} h_{\text{ref}} \\ L_{\text{ref}} \end{bmatrix} - A_j(q_{\text{ref}})\dot{q}_{\text{ref}}^j \right) \quad (7)$$

where $A(q)$ is partitioned as $A(q) := [A_b(q), A_j(q)]$ with $A_b(q) \in \mathbb{R}^{6 \times 6}$. Partition the matrix $D(q)$ in (1) as

$$D(q) = \begin{bmatrix} D_{11}(q) & D_{12}(q) \\ D_{21}(q) & D_{22}(q) \end{bmatrix} \quad (8)$$

where $D_{11}(q) \in \mathbb{R}^{6 \times 6}$. The reference acceleration vector for the actuated joints $\ddot{q}_{\text{ref}}^j \in \mathbb{R}^n$ is obtained by directly differen-

tiating the joint velocity \dot{q}_{ref}^j . The base reference acceleration \ddot{q}_{ref}^b for the base can be calculated as follows

$$\ddot{q}_{\text{ref}}^b = D_{11}(q_{\text{ref}})^{-1} (S_\theta(-C(\dot{q}_{\text{ref}}, q_{\text{ref}})\dot{q}_{\text{ref}} - G(q_{\text{ref}}) + J^\top F_{\text{ref}} - D_{12}(q_{\text{ref}})\ddot{q}_{\text{ref}}^j)).$$

where $S_\theta = [I_6, 0_{6 \times n}]$. The reference acceleration is given by

$$\ddot{q}_{\text{ref}} = \begin{bmatrix} \ddot{q}_{\text{ref}}^b \\ \ddot{q}_{\text{ref}}^j \end{bmatrix}. \quad (9)$$

The input reference trajectory can be obtained by

$$\tau_{\text{ref}} = S(D(q_{\text{ref}})\ddot{q}_{\text{ref}} + C(q_{\text{ref}}, \dot{q}_{\text{ref}})\dot{q}_{\text{ref}} + G(q_{\text{ref}}) - J^\top F_{\text{ref}})$$

where S is given in (1).

IV. ADAPTIVE EXTENDED STATE DISTURBANCES ESTIMATOR

In this section, we first rewrite the whole-body dynamics (1) and then introduce the model of uncertainties.

In (1), the first six rows represent the unactuated dynamics, while the remaining rows correspond to the actuated dynamics. Let $x_1 = q$ and $x_2 = \dot{q}$. The dynamics model can be written in the state-space form

$$\begin{bmatrix} \dot{x}_1 \\ \dot{x}_2 \end{bmatrix} = \begin{bmatrix} x_2 \\ f_0(x_1, x_2) \end{bmatrix} + \begin{bmatrix} 0 \\ g_0(x_1) \end{bmatrix} u + \begin{bmatrix} 0 \\ \bar{d} \end{bmatrix} \quad (10)$$

where $\bar{d} := D^{-1}(x_1)d$,

$$\begin{aligned} f_0(x_1, x_2) &:= -D^{-1}(x_1)(C(x_2, x_1)x_2 + G(x_1)) \\ g_0(x_1) &:= D^{-1}(x_1)B \end{aligned} \quad (11)$$

with $B = [S^\top, J(q)^\top]$ and $u = [\tau^\top, F^\top]^\top$.

The uncertainties mostly come from inaccurate modeling for mass and inertia, and the impact of different terrains on the robot is also unknown. Inspired by [5], the modeling uncertainties can be handled by the PD control law with the appropriate controller parameters. As in [5], without directly modeling the uncertainty, we propose the uncertainty in terms of a PD term with unknown parameters as follows

$$d_1(e, t) = E_q \theta \quad (12)$$

where $d_1 \in \mathbb{R}^n$, $\theta \in \mathbb{R}^{2n}$ are unknown parameters that need to be estimated and $E_q = \{\text{diag}\{e_q^\top\}, \text{diag}\{\dot{e}_q^\top\}\} \in \mathbb{R}^{n \times 2n}$ with $e_q = q_{\text{ref}}^j - q^j$ and $\dot{e}_q = \dot{q}_{\text{ref}}^j - \dot{q}^j$ where both the desired joint position q_{ref}^j and joint velocity \dot{q}_{ref}^j are calculated by solving MPC problem (5), and q^j and \dot{q}^j are joint position and velocity of the legged robot, respectively. The estimated parameter θ acts as PD controller parameters, while the uncertainty d_1 serves as the controller output to adjust the robot's joint stiffness, thereby enhancing its robustness. In addition to the uncertainty d_1 in the actuated dynamics, we introduce the additive uncertainty $d_2(t) \in \mathbb{R}^{6+n}$ in the unactuated dynamics and the uncertainty term d is

$$\bar{d}(e, t) = S^\top d_1(e, t) + d_2(t). \quad (13)$$

As stated in [6], handling the uncertainty term d_2 would greatly improve the disturbance rejection performance especially when the foot contact force estimation is inaccurate.

To estimate the uncertainty d , recall the dynamics (1) as follows:

$$\begin{bmatrix} \dot{x}_1 \\ \dot{x}_2 \end{bmatrix} = \begin{bmatrix} x_2 \\ f_0(x_1, x_2) \end{bmatrix} + \begin{bmatrix} 0 \\ g_0(x_1) \end{bmatrix} u + \begin{bmatrix} 0 \\ S^\top E_q \theta + d_2(t) \end{bmatrix}. \quad (14)$$

Note that there exist unknown parameters θ in d_1 , as well as nonlinearities d_2 , in the uncertainty d . We aim to propose a general whole-body disturbance rejection scheme to estimate the uncertainty in legged robot systems. To achieve this, we combine adaptive control, which is used to estimate the unknown parameters, with ESO used to estimate the nonlinearities, utilizing full-state feedback in a single unified controller. In this approach, the uncertain nonlinearities are handled simultaneously.

A. Projection Mapping and Parameter Adaptation

Assumption 4.1: The defined parameter set θ satisfies

$$\theta \in \Omega_\theta \triangleq \{\theta = [\theta_i] : \theta_{i \min} \leq \theta_i \leq \theta_{i \max}\} \quad (15)$$

where $\theta_{\min} = [\theta_{1 \min}, \dots, \theta_{(2n) \min}]^\top$ and $\theta_{\max} = [\theta_{1 \max}, \dots, \theta_{(2n) \max}]^\top$ are known. ■

Let $\hat{\theta}$ denote the estimate of θ and $\tilde{\theta}$ the estimation error (i.e., $\tilde{\theta} = \theta - \hat{\theta}$). A discontinuous projection can be defined as

$$\text{Proj}_{\hat{\theta}_i}(\bullet_i) = \begin{cases} 0, & \text{if } \hat{\theta}_i = \theta_{i \max} \text{ and } \bullet_i > 0 \\ 0, & \text{if } \hat{\theta}_i = \theta_{i \min} \text{ and } \bullet_i < 0 \\ \bullet_i, & \text{otherwise} \end{cases} \quad (16)$$

where $i = 1, \dots, 2n$. By using an adaptation law given by

$$\dot{\hat{\theta}} = \text{Proj}_{\hat{\theta}}(\Gamma \alpha) \quad \text{with } \theta_{\min} \leq \hat{\theta}(0) \leq \theta_{\max} \quad (17)$$

where $\text{Proj}_{\hat{\theta}}(\Gamma \alpha) = [\text{Proj}_{\hat{\theta}_0}(\Gamma_0 \alpha), \dots, \text{Proj}_{\hat{\theta}_{2n}}(\Gamma_{2n} \alpha)]^\top$, $\Gamma > 0$ is a diagonal matrix of the adaptation rate and Γ_i represents the i -th row of the matrix Γ , and α is an adaptation function to be synthesized later; for any adaptation function α , the projection mapping guarantees [20]

$$\begin{aligned} \hat{\theta} &\in \Omega_{\hat{\theta}} \triangleq \{\hat{\theta} : \theta_{\min} \leq \hat{\theta} \leq \theta_{\max}\} \\ \tilde{\theta}^\top [\Gamma^{-1} \text{Proj}_{\hat{\theta}}(\Gamma \alpha) + \alpha] &\leq 0, \forall \alpha. \end{aligned} \quad (18)$$

The adaptation rate Γ controls the balance between responsiveness and stability, with a higher rate enabling quicker adjustments at the cost of stability, and a lower rate ensuring stability but slower responsiveness.

B. ESO Design

We introduce the extended state $x_3 \in \mathbb{R}^{6+n}$ as $x_3 = d_2$ and h denote the rate of change of x_3 , i.e., $h = \dot{x}_3$. Both x_3 and h are assumed to be unknown but bounded signal vectors. The system (14) can be expressed in a state-space form as

$$\begin{cases} \dot{x}_1 = x_2 \\ \dot{x}_2 = f_0(x_1, x_2) + g_0(x_1)u + S^\top E_q \theta + x_3 \\ \dot{x}_3 = h(t) \end{cases} \quad (19)$$

Remark 4.1: There exists another way to define the extend state x_3 , as $x_3 = S^\top E_q \tilde{\theta} + d_2(t)$. Then, the system (14) can be rewritten as

$$\begin{cases} \dot{x}_1 = x_2 \\ \dot{x}_2 = f_0(x_1, x_2) + g_0(x_1)u + S^\top E_q \tilde{\theta} + x_3 \\ \dot{x}_3 = h(t) \end{cases}$$

It is worth noting that, the two definitions of the extended states do not affect the ESO to be constructed later. Although the dynamics of the state estimation errors will be different, the subsequent stability analysis and conclusions remain the same. ■

Let \hat{x}_1 , \hat{x}_2 , and \hat{x}_3 be the estimate of x_1 , x_2 and x_3 , respectively. By referring to [21], the linear ESO can be constructed as follows:

$$\begin{cases} \dot{\hat{x}}_1 = \hat{x}_2 + 3\omega_0(x_1 - \hat{x}_1) \\ \dot{\hat{x}}_2 = f_0(x_1, x_2) + g_0(x_1)\hat{u} + S^\top E_q \tilde{\theta} + \hat{x}_3 + 3\omega_0^2(x_1 - \hat{x}_1) \\ \dot{\hat{x}}_3 = \omega_0^3(x_1 - \hat{x}_1) \end{cases} \quad (20)$$

where $\hat{u} = [F_{\text{ref}}^\top, \tau^\top]^\top$ with F_{ref} being obtained by solving the MPC problem (5), and ω_0 are tuning parameters to be determined. The parameter ω_0 affects the bandwidths of the ESO. While a large ω_0 is necessary for fast disturbance estimation, it can also amplify noise. Due to the absence of ground reaction force sensors on the legged robot, we use F_{ref} in \hat{u} to replace the actual GRFs F in u , and the discrepancy between F and F_{ref} is estimated by ESO. Note that if the legged robot operates without uncertainty, and the robot's position q and velocity \dot{q} perfectly track q_{ref} and \dot{q}_{ref} , then \hat{u} will be equal to u , i.e., $u - \hat{u} = 0$. For the ESO in (20), the system state x and system input τ in \hat{u} can be directly measured or obtained by state estimation, while $\tilde{\theta}$ is computed using the adaptation law (17).

Next, we will analyze the stability of the proposed ESO. Let

$$\eta = [(x_1 - \hat{x}_1)^\top, (x_2 - \hat{x}_2)^\top / \omega_0, (x_3 - \hat{x}_3)^\top / \omega_0^2]^\top \quad (21)$$

be the state estimation error and $\tilde{u} = u - \hat{u}$. The dynamics of the state estimation errors can be expressed as

$$\dot{\eta} = \omega_0 A \eta + \frac{C_1(g_0(x_1)\tilde{u} + S^\top E_q \tilde{\theta})}{\omega_0} + \frac{C_2 h(t)}{\omega_0^2} \quad (22)$$

where $\tilde{u} = u - \hat{u}$ is an unknown but bounded vector, since $\|\tilde{u}\| = \|F - F_{\text{ref}}\|$, with F_{ref} being bounded as a result of solving MPC problem (5), $g_0(x_1)$ is a bounded matrix, and

$$\begin{aligned} A &= \begin{bmatrix} -3 & 1 & 0 \\ -3 & 0 & 1 \\ -1 & 0 & 0 \end{bmatrix} \otimes I_{6+n}, \quad C_1 = \begin{bmatrix} 0 \\ 1 \\ 0 \end{bmatrix} \otimes I_{6+n}, \\ C_2 &= \begin{bmatrix} 0 \\ 0 \\ 1 \end{bmatrix} \otimes I_{6+n}. \end{aligned} \quad (23)$$

Theorem 4.1: Consider the error dynamics (22) and adaptation dynamics (17) under Assumption 4.1 where the adaptation function α is

$$\alpha = \frac{E_q^\top S C_1^\top P \eta}{\omega_0} \quad (24)$$

with ESO bandwidth parameter $\omega_0 > 0$ and matrix P satisfying $A^\top P + PA = -I$. Suppose there is no uncertainty, i.e., $x_3 = 0$ and $h = 0$. When the robot's state $x = \text{col}(q, \dot{q})$ perfectly tracks the reference trajectory $x_{\text{ref}} = \text{col}(q_{\text{ref}}, \dot{q}_{\text{ref}})$ derived from the MPC problem (5), i.e., $\tilde{u} = 0$, one has $\lim_{t \rightarrow \infty} (x - \hat{x}) = 0$. ■

Proof: Let us consider the following control Lyapunov candidate function:

$$V(\eta, \tilde{\theta}) = \eta^\top P \eta + \tilde{\theta}^\top \Gamma^{-1} \tilde{\theta}. \quad (25)$$

Therefore, its time derivative will be

$$\begin{aligned} \dot{V}(\eta, \tilde{\theta}) &= -\omega_0 \|\eta\|^2 + \tilde{\theta}^\top (\Gamma^{-1} \dot{\tilde{\theta}} + \frac{E_q^\top S C_1^\top P \eta}{\omega_0}) \\ &\quad + (\dot{\tilde{\theta}}^\top \Gamma^{-1} + \frac{\eta^\top P C_1 S^\top E_q}{\omega_0}) \tilde{\theta} + \frac{\tilde{u}^\top g_0^\top C_1^\top P \eta + \eta^\top P C_1 g_0 \tilde{u}}{\omega_0} \\ &\quad + \frac{h^\top C_2^\top P \eta + \eta^\top P C_2 h}{\omega_0^2}. \end{aligned} \quad (26)$$

Combining the adaptation law (24) and (26), we have

$$\dot{V}(\eta, \tilde{\theta}) = -\omega_0 \|\eta\|^2. \quad (27)$$

Combining (25) and (27), it gives η and $\tilde{\theta}$ are bounded. According to (22), we have $\dot{\eta}$ is bounded. Using Barbalat Lemma, (27) implies $\lim_{t \rightarrow \infty} (x - \hat{x}) = 0$. ■

Theorem 4.2: Consider the error dynamics (22) and adaptation dynamics (17) under Assumption 4.1 where the adaptation function α is

$$\alpha = \frac{E_q^\top S C_1^\top P \bar{\eta}}{\omega_0}$$

where $\omega_0 > 0$, $\bar{\eta} = [(x_1 - \hat{x}_1)^\top, (x_2 - \hat{x}_2)^\top / \omega_0, -\hat{x}_3^\top / \omega_0^2]^\top$, and the matrix P satisfying $A^\top P + PA = -I$, $\|\tilde{\theta}\| < \tilde{\theta}_b$. Suppose both the disturbance x_3 and its derivative h are bounded, i.e., $\|x_3\| \leq d_b$ and $\|h\| < h_b$. If both the matrix E_q and the error vector $g_0 \tilde{u}$ are bounded, i.e., $\|E_q\| < e_b$, $\|g_0 \tilde{u}\| \leq \tilde{u}_b$, then the estimation error η is bounded. ■

Proof: By Assumption 4.1 and property of the projection operators, the projection operators will keep $\tilde{\theta}$ bounded. We have these bounds as $\|\tilde{\theta}\| < \tilde{\theta}_b$. From (25), we have

$$V(\eta, \tilde{\theta}) \leq \lambda_{\max}(P) \|\eta\|^2 + \|\Gamma\|^{-1} \tilde{\theta}_b^2 \quad (28)$$

with $\lambda_{\max}(P)$ being the maximum eigenvalue of matrix P . From (26), we have

$$\begin{aligned} \dot{V}(\eta, \tilde{\theta}) &\leq -\omega_0 \|\eta\|^2 + \left(\frac{2\tilde{u}_b \|C_1^\top P\|}{\omega_0} + \frac{2h_b \|C_2^\top P\|}{\omega_0^2} \right) \|\eta\| \\ &\quad + \frac{2\|S C_1^\top P\| e_b d_b \tilde{\theta}_b}{\omega_0^3}. \end{aligned} \quad (29)$$

Let $\lambda = \omega_0 / (2\lambda_{\max}(P))$. Combining (28) and (29), we have

$$\dot{V}(\eta, \tilde{\theta}) + \lambda V(\eta, \tilde{\theta}) \leq a(\|\eta\| + \frac{b}{2})^2 + \lambda \delta_V \quad (30)$$

where

$$a = -\omega_0 + \lambda \lambda_{\max}(P), \quad b = 2 \left(\frac{\tilde{u}_b \|C_1^\top P\|}{\omega_0} + \frac{h_b \|C_2^\top P\|}{\omega_0^2} \right) / a,$$

$$\delta_V = \frac{2(\omega_0 \tilde{u}_b \|C_1^\top P\| + h_b \|C_2^\top P\|)^2}{\lambda \omega_0^5} + \frac{2\|SC_1^\top P\| e_b d_b \tilde{\theta}_b}{\lambda \omega_0^3} + \|\Gamma\|^{-1} \tilde{\theta}_b.$$

From (30), we have

$$\dot{V}(\eta, \tilde{\theta}) + \lambda V(\eta, \tilde{\theta}) \leq \lambda \delta_V. \quad (31)$$

It follows that

$$V(\eta, \tilde{\theta}) \leq V(\eta_0, \tilde{\theta}_0) \exp(-\lambda t) + \delta_V (1 - \exp(-\lambda t))$$

where η_0 and $\tilde{\theta}_0$ are the values of η and $\tilde{\theta}$, respectively.

Since $V(\eta, \tilde{\theta}) \geq \lambda_{\min}(P) \|\eta\|^2$, with $\lambda_{\min}(P)$ being the minimum eigenvalue of matrix P , it follows that

$$\|\eta\| \leq \sqrt{\frac{V(\eta_0, \tilde{\theta}_0) \exp(-\lambda t) + \delta_V (1 - \exp(-\lambda t))}{\lambda_{\min}(P)}}.$$

Thus, the estimation error η is bounded. \blacksquare

V. DISTURBANCE REJECTION WHOLE BODY PLANNER

The uncertainty of the robot system is estimated in Section IV-B. In this section, we will focus on compensating for the uncertainty in the robot system by using a quadratic programming and WBC framework (QP-WBC).

To reduce the noise, we applied a moving average filter (MAF) to smooth the estimated uncertainty. The estimated uncertainty given by the adaptive ESO is

$$\hat{f} = D(x_1)(\hat{x}_3 + S^\top E_q \hat{\theta}). \quad (32)$$

Let \hat{f}_{filter} be the moving average filtered value of \hat{f} at this moment.

Next, we use the hierarchical WBC to address uncertainties in the legged system. A detailed formulation of the WBC can be found in [22]. Each task within the WBC is represented as an equality constraint or an inequality constraint on generalized accelerations, joint actuation torques, and GRFs. Define the desired wrench of the robot as

$$W_d^* = \hat{f}_{\text{filter}} + J(q_{\text{ref}})^\top F_{\text{ref}} + S^\top \tau_{\text{ref}} \quad (33)$$

which is the value of the right-hand side of the equation in dynamics (1) when the robot's position, velocity, and acceleration perfectly track the corresponding reference values and the disturbance is well estimated. To formulate the WBC problem, the dynamic constraint in WBC is expressed as:

$$D(q)\ddot{q}_d + C(q, \dot{q})\dot{q} + G(q) = W_d^* \quad (34)$$

where \ddot{q}_d represents the optimal acceleration required in the WBC, and q and \dot{q} are the measured joint position and velocity. The GRFs of the legged robot vary with changes in uncertainty, meaning that we cannot directly use the reference GRFs F_{ref} obtained from the MPC problem based on the ideal dynamics, to optimize the GRFs in the WBC. Inspired by the method in [6] for calculating GRFs with uncertainty in legged

robots, we formulate a QP problem to obtain the desired GRFs F_r^* :

$$\begin{aligned} & \min_{\tau_r, F_r} \frac{1}{2} \|F_r - F_{\text{ref}}\|_{Q_1}^2 + \frac{1}{2} \|J(q_{\text{ref}})^\top F_r + S^\top \tau_r - W_d^*\|_{Q_2}^2 \\ & \text{s.t.} \quad C_f F_r \leq 0 \end{aligned} \quad (35)$$

where C_f is the contact constraint matrix, and Q_1 and Q_2 are the weight matrices for these two objectives respectively. In this QP problem (35), we obtain the desired GRFs F_r^* to ensure that the wrench of the legged robot, without uncertainty (i.e., the right-hand side of the dynamics equation (1) with $d = 0$), matches the desired wrench W_d^* , with F_r^* approximating the reference GRFs F_{ref} . Let $\hat{f}_{\text{filter}}^w = \hat{f}_{\text{filter}} - J(q_{\text{ref}})^\top (F_r^* - F_{\text{ref}})$, where F_r^* corresponds to the solution of the QP.

Then, the desired wrench (33) can be rewritten as

$$W_d^* = J(q_{\text{ref}})^\top F_r^* + S^\top \tau_{\text{ref}} + \hat{f}_{\text{filter}}^w. \quad (36)$$

Note that the wrench in (33) is equivalent to that in (36). The difference lies in the introduction of the GRFs F_r^* , given by (36), which are used for tracking in the WBC, a feature not present in (33). These desired GRFs F_r^* will later serve as the foot-end force tracking constraint in the designed WBC, while $\hat{f}_{\text{filter}}^w$ obtained by (36) will serve as dynamics constraint.

The WBC can be formulated as

$$\begin{aligned} & \text{find } \ddot{q}_d, F_d, \tau_d \\ & \text{s.t.} \quad \underline{u} \leq u \leq \bar{u} \quad (\text{Torque limits}) \\ & \quad D(q)\ddot{q}_d + C(q, \dot{q})\dot{q} + G(q) = S^\top \tau_d + J(q)^\top F_d + \hat{f}_{\text{filter}}^w \quad (\text{Dynamics}) \\ & \quad J(q)\ddot{q}_d + \dot{J}(q)\dot{q} = 0 \quad (\text{No motion for contact foots}) \\ & \quad C_f F_d \leq 0 \quad (\text{Friction cone}) \\ & \quad S_w F_d = 0 \quad (\text{No wrench for swing foots}) \\ & \quad \ddot{q}_d - \ddot{q}_{\text{ref}} = 0 \quad (\text{Acceleration tracking}) \\ & \quad F_d - F_r^* = 0 \quad (\text{Foot-end force tracking}) \end{aligned}$$

where \underline{u} and \bar{u} represent the lower and upper limits of the torque, q and \dot{q} are measured joint position and velocity, S_w is the swing leg selection matrix ensuring that the contact forces of the swing leg are selected. \ddot{q}_{ref} represents the desired acceleration and is calculated in (9). Tasks are solved in a strict prioritized order. The priority of tasks is described in Table I. Finally, the actuation joint torque u_d can be computed using the PD control law as follows:

$$u_d = \tau_d^* + K_p (q_{\text{ref}}^j - q^j) + K_d (\dot{q}_{\text{ref}}^j - \dot{q}^j) \quad (37)$$

where τ_d^* is obtained by solving WBC problem, $K_p \in \mathbb{R}^{n \times n}$ and $K_d \in \mathbb{R}^{n \times n}$ are positive-define diagonal matrices of proportional and derivative gains, respectively, q_{ref}^j and \dot{q}_{ref}^j are the bottom n rows of q_{ref} and \dot{q}_{ref} , respectively.

TABLE I: Priority of Tasks

| Priority | Task |
|----------|---|
| 1 | Dynamics + Friction cone + No wrench for swings + Torque limits |
| 2 | Acceleration tracking |
| 3 | No motion for contact foots + Foot-end force tracking |

VI. SIMULATION COMPARISON

To assess the effectiveness and versatility of the WB-DRC, we conduct a series of simulation experiments on legged robots and compare the performance of the proposed WB-DRC with the widely adopted standard WBC from [18]. All simulations are performed on a single PC (Intel i7-13700KF, 3.4 GHz). For the simulations, the control system is implemented using ROS Noetic in the Gazebo simulator. The simulations are carried out on both a biped robot, which has $n = 12$ degrees of actuation freedom, and the Unitree A1 quadruped robot, which also has $n = 12$ degrees of actuation freedom. The biped robot simulation is detailed in Section VI-A, while the quadruped robot simulation is described in Section VI-B.

A. Simulation on Biped Robot

The operating frequency of the MPC is 50Hz, with a prediction horizon $T = 1$ s and the total number of steps $N = 30$, while the operating frequency of the adaptive ESO and QP-WBC are 1000Hz. The sliding window width of the MAF is set to 7. The control parameters for the WB-DRC are specified in Table II. The desired height of base link (see Fig. 3) is set to 0.86 m. To verify the robustness of the proposed WB-DRC and the effectiveness of the disturbance estimator, we simulated a scenario in Gazebo by deliberately reducing the knee joint torque by 30%. The standing pose with the WB-DRC and that with the standard WBC in simulation environment are shown in Fig. 3. It demonstrates that the biped robot is capable of handling output torque reduction through WB-DRC. The estimation parameters $\hat{\theta}$ for the robot in WB-DRC using the adaptation law are presented in Fig. 4. All estimated values, $\hat{\theta}_{13} \sim \hat{\theta}_{24}$, remain bounded within the interval $[-100, 100]$.

Fig. 5 illustrates the height of the base link from the ground over time as the robot performs the stepping in place with an 8 kg load, from 4 s to 20 s. The results show that the base link height of the biped robot using WB-DRC closely tracks the desired height. However, the robot with the standard WBC does not tracks the desired height and falls to the ground at around 14s. Similarly, Fig. 6 shows the base link height as the robot walks with a 6 kg load at 8 s. It shows that the robot using the standard WBC falls at around 16 s. These results suggest that the biped robot with WB-DRC is more robust to the model uncertainty than the robot with the standard WBC.

TABLE II: WB-DRC Setting

| Parameter | Value for Biped Robot | Value for Quadruped Robot |
|-------------------|--|---|
| Γ | $50000 \times I_{24 \times 24}$ | $6 \times 10^5 \times I_{24 \times 24}$ |
| ω_0 | 100 | 350 |
| $\hat{\theta}(0)$ | $\mathbf{0}_{24 \times 1}$ | $\mathbf{0}_{24 \times 1}$ |
| θ_{\max} | $100 \times \mathbf{1}_{24 \times 1}$ | $100 \times \mathbf{1}_{24 \times 1}$ |
| θ_{\min} | $-100 \times \mathbf{1}_{24 \times 1}$ | $-100 \times \mathbf{1}_{24 \times 1}$ |
| Q_1 | $100 \times I_{24 \times 24}$ | $100 \times I_{24 \times 24}$ |
| Q_2 | $I_{18 \times 18}$ | $I_{18 \times 18}$ |
| K_p | $15 \times I_{12 \times 12}$ | $0 \times I_{12 \times 12}$ |
| K_d | $0.5 \times I_{12 \times 12}$ | $3 \times I_{12 \times 12}$ |

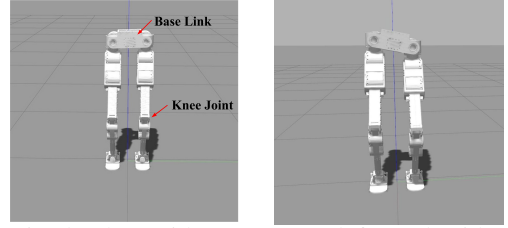


Fig. 3: Biped robot with WB-DRC (left) and with standard WBC (right) in a simulation environment.

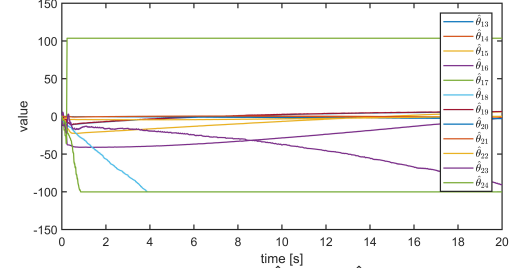


Fig. 4: The estimation value $\hat{\theta}_{13} \sim \hat{\theta}_{24}$ using adaptive law when the output torque of the robot knee joint is reduced by 30%.

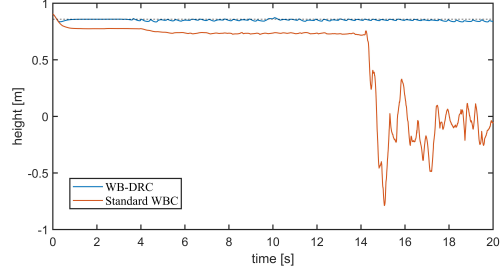


Fig. 5: The height of the base link from the ground over time as the robot performs stepping in place with an 8 kg load.

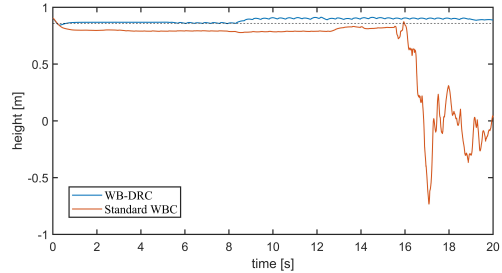


Fig. 6: The height of the base link from the ground over time as the robot walks with an 6 kg load.

B. Simulation on Quadruped Robot

The operating frequency of the MPC is 20Hz with a prediction horizon $T = 1$ s and the total number of steps $N = 30$, and the running frequency of the adaptive ESO and QP-WBC are 1000 Hz. The sliding window width of MAF is set to 3. We set the control parameters for WB-DRC as presented in Table II. To assess the performance of the proposed WB-DRC, two simulation studies are carried out. The first study involves applying an external force along the z -axis to the robot's center of base link (see Fig. 7). In the second study, we simulate the robot walking while carrying an 8 kg load, which accounts for up to 60% of its body weight.

The desired height of the base link is 0.31 m. Fig. 8 shows

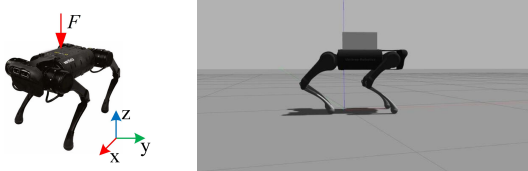


Fig. 7: The Unitree A1 robot (left) and its model in the simulation environment with an 8 kg load (right).

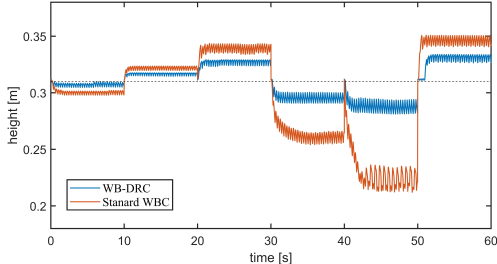


Fig. 8: The height of the base link from the ground over time under the application of different external forces.

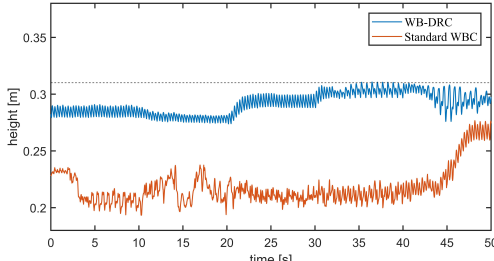


Fig. 9: The height of the base link from the ground over time as the robot moves at different velocities with 8kg load.

the height of the base link from the ground over time under the influence of various constant external forces. External forces of -20 N, 20 N, 60 N, -60 N, -80 N, and 80 N are applied to the base link along the z -axis, each for a duration of 10 seconds. The results demonstrate that the proposed WB-DRC compensates for these external disturbances better than the standard WBC. Fig. 9 illustrates the height of the base link over time as the robot with 8 kg load walks at different velocities along the x -axis. The robot is commanded to move on the flat ground with velocities of -0.1 m/s, 0.1 m/s, 0.2 m/s, 0.4 m/s, and 0.6 m/s, each for a duration of 10 seconds. The results demonstrate that the WB-DRC maintains the body height closer to the 0.31 m, showing its capability to effectively handle model uncertainties.

VII. EXPERIMENT COMPARISON

We conduct two real-robot experiments on the Unitree A1 quadruped robot. In the first experiment, we simulate the motor malfunction by decreasing joint motor torque, and in the second experiment we compare the performance of WB-DRC and standard WBC under the same load. The control architecture is implemented on a PC (Intel i7-13700KF, 3.4 GHz). The MPC operates at a frequency of 100 Hz, with a prediction horizon $T = 1$ s and the total number of steps $N = 30$, while both the adaptive ESO and QP-WBC run at 1000 Hz. The sliding window for the MAF is set to 5. The

controller parameters for the WB-DRC are provided in Table III. The desired base link height is set to 0.3 m.

First, we intentionally reduce the output torque of the robot knee joint on the right back leg by 50%. The base link height of the robot, when the robot switches from standing to stepping in place, is shown in Fig. 10 for WB-DRC and standard WBC. For WB-DRC, the height trajectory of the base link closely follows the desired trajectories, outperforming the robot using the standard WBC. Second, we intentionally reduce both the output torque of the robot's knee joint and the output torque of the robot's hip joint on the right back leg by 60% at 11s, with a duration of 1s, and by 90% at 15.8s, with a duration of 0.2s. The base link height of the robot is shown in Fig. 11 for WB-DRC and standard WBC. The base link height of the robot using WB-DRC is less affected by short-term motor torque output failure than the robot using standard WBC. As shown in Figs. 10 through 11, the robot using the WB-DRC exhibits better fault tolerance and enhanced robustness compared to the robot using the standard WBC.

TABLE III: WB-DRC Setting

| Parameter | Value | Parameter | Value |
|-------------------|--|-----------|-------------------------------|
| Γ | $6000 \times I_{24 \times 24}$ | Q_1 | $500 \times I_{24 \times 24}$ |
| ω_0 | 200 | Q_2 | $I_{18 \times 18}$ |
| $\hat{\theta}(0)$ | $\mathbf{0}_{24 \times 1}$ | K_p | $0 \times I_{12 \times 12}$ |
| θ_{\max} | $100 \times \mathbf{1}_{24 \times 1}$ | K_d | $3 \times I_{12 \times 12}$ |
| θ_{\min} | $-100 \times \mathbf{1}_{24 \times 1}$ | | |

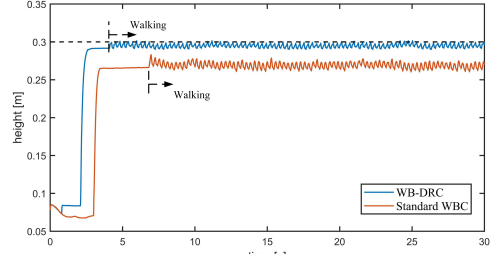


Fig. 10: The base link height of the robot from standing to stepping in place.

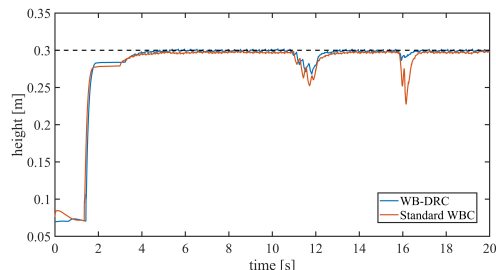


Fig. 11: The base link height of the robot from standing to stepping in place.

To further evaluate the performance of WB-DRC, we conducted the experiment where the robot carries a 5 kg load. Fig. 12 illustrates the height of the robot's base link under both WB-DRC and standard WBC. The robot using the standard WBC falls at around 6 s, as shown in Fig. 13, while the robot with the proposed WB-DRC is able to walk continuously for the full 20 seconds. We performed three consecutive tests on the robot carrying a 5 kg load using the

standard WBC. The results, shown in Fig. 14, indicate that the standard WBC is unable to effectively handle the robot's 5 kg load, whereas the WB-DRC performs successfully. These experiments demonstrate that the WB-DRC offers significant advantages in terms of robustness and stability.

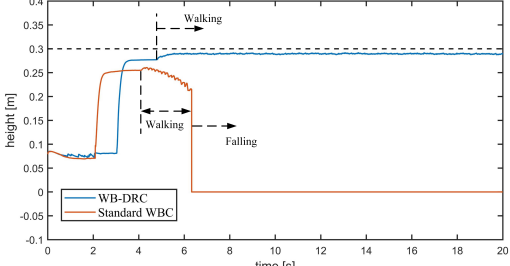


Fig. 12: The height of the base link when the robot using WB-DRC and standard WBC walks with 5 kg load.



Fig. 13: The Unitree A1 robot using standard WBC falls at around 6 s.

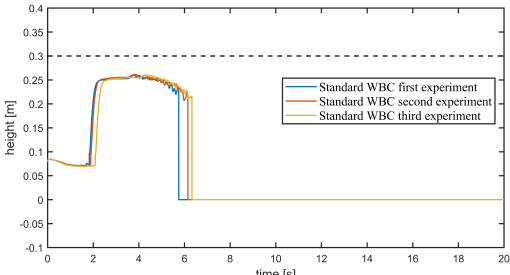


Fig. 14: The height of the base link when the robot using standard WBC walks with 5 kg load.

To demonstrate the capability of the control framework in handling model uncertainties and external disturbances on rough terrain, we conduct a real robot experiment on challenging terrain. As shown in Fig. 15, the robot successfully navigates the rough terrain at significant velocity while carrying a 5 kg load, highlighting the effectiveness of the proposed framework in enabling the robot to traverse difficult environments.

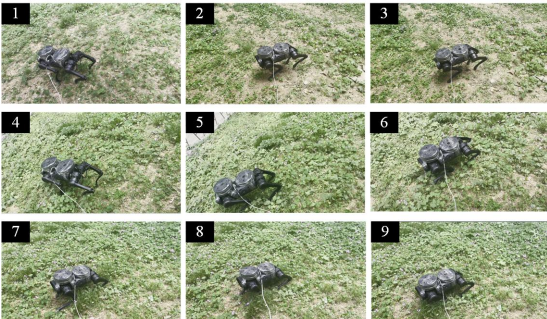


Fig. 15: The robot moves on tough terrain while carrying a 5 kg load.

VIII. CONCLUSIONS

In this letter, we present a novel control framework for legged robots that enhances self-perception and robustness against external disturbances and model uncertainties. The proposed disturbance estimator, which combines adaptive control with an ESO, effectively estimates and compensates for disturbances and uncertainties within the whole-body control framework. The WB-DRC improves the robot's ability to handle various uncertainties, particularly those related to joint motor output torque inaccuracies, while also expanding the application range, making it suitable not only for quadruped robots but also for biped humanoid robots, surpassing traditional methods. Simulation results for both biped and quadruped robots, along with experiments on the Unitree A1 quadruped, demonstrate the framework's effectiveness, robustness, and stability. This research offers a promising solution for enhancing the performance of legged robots in dynamic environments.

REFERENCES

- [1] S. Fahmi, V. Barasuol, D. Esteban, O. Villarreal, and C. Semini, "Vital: Vision-based terrain-aware locomotion for legged robots," *IEEE Transactions on Robotics*, vol. 39, no. 2, pp. 885–904, 2023.
- [2] D. G. E. Hobbelen and M. Wisse, "Swing-leg retraction for limit cycle walkers improves disturbance rejection," *IEEE Transactions on Robotics*, vol. 24, no. 2, pp. 377–389, 2008.
- [3] B. Li, L. Zhu, and J. Huang, "Stable locomotion of biped robot with gaits of sinusoidal harmonics," *IEEE Transactions on Control Systems Technology*, vol. 32, no. 3, pp. 805–817, 2024.
- [4] S. Xu, L. Zhu, H.-T. Zhang, and C. P. Ho, "Robust convex model predictive control for quadruped locomotion under uncertainties," *IEEE Transactions on Robotics*, vol. 39, no. 6, pp. 4837–4854, 2023.
- [5] M. Sombolostan and Q. Nguyen, "Adaptive force-based control of dynamic legged locomotion over uneven terrain," *IEEE Transactions on Robotics*, 2024.
- [6] Z. Zhu, G. Zhang, Z. Sun, T. Chen, X. Rong, A. Xie, and Y. Li, "Proprioceptive-based whole-body disturbance rejection control for dynamic motions in legged robots," *IEEE Robotics and Automation Letters*, 2023.
- [7] A. De Luca and F. Flacco, "Integrated control for phri: Collision avoidance, detection, reaction and collaboration," in *2012 4th IEEE RAS and EMBS International Conference on Biomedical Robotics and Biomechatronics (BioRob)*, 2012, pp. 288–295.
- [8] G. Bledt, P. M. Wensing, S. Ingersoll, and S. Kim, "Contact model fusion for event-based locomotion in unstructured terrains," in *2018 IEEE International Conference on Robotics and Automation (ICRA)*, 2018, pp. 4399–4406.
- [9] V. Morlando, A. Teimoorzadeh, and F. Ruggiero, "Whole-body control with disturbance rejection through a momentum-based observer for quadruped robots," *Mechanism and Machine Theory*, vol. 164, p. 104412, 2021.
- [10] L. Amanzadeh, T. Chunawala, R. T. Fawcett, A. Leonessa, and K. A. Hamed, "Predictive control with indirect adaptive laws for payload transportation by quadrupedal robots," *IEEE Robotics and Automation Letters*, vol. 9, no. 11, pp. 10 359–10 366, 2024.
- [11] J. Han, "From pid to active disturbance rejection control," *IEEE Transactions on Industrial Electronics*, vol. 56, no. 3, pp. 900–906, 2009.
- [12] M. Ran, J. Li, and L. Xie, "A new extended state observer for uncertain nonlinear systems," *Automatica*, vol. 131, p. 109772, 2021.
- [13] B. Li, L. Zhu, and Z. Chen, "An improved active disturbance rejection control for bode's ideal transfer function," *IEEE Transactions on Industrial Electronics*, vol. 71, no. 7, pp. 7673–7683, 2024.
- [14] J. Yao and W. Deng, "Active disturbance rejection adaptive control of hydraulic servo systems," *IEEE Transactions on Industrial Electronics*, vol. 64, no. 10, pp. 8023–8032, 2017.
- [15] J. Carpenter and N. Mansard, "Multicontact locomotion of legged robots," *IEEE Transactions on Robotics*, vol. 34, no. 6, pp. 1441–1460, 2018.

- [16] D. E. Orin and A. Goswami, “Centroidal momentum matrix of a humanoid robot: Structure and properties,” in 2008 IEEE/RSJ International Conference on Intelligent Robots and Systems. IEEE, 2008, pp. 653–659.
- [17] G. Bledt, M. J. Powell, B. Katz, J. Di Carlo, P. M. Wensing, and S. Kim, “Mit cheetah 3: Design and control of a robust, dynamic quadruped robot,” in 2018 IEEE/RSJ International Conference on Intelligent Robots and Systems (IROS), 2018, pp. 2245–2252.
- [18] R. Grandia, F. Jeneften, S. Yang, F. Farshidian, and M. Hutter, “Perceptual locomotion through nonlinear model-predictive control,” IEEE Transactions on Robotics, vol. 39, no. 5, pp. 3402–3421, 2023.
- [19] D. E. Orin, A. Goswami, and S.-H. Lee, “Centroidal dynamics of a humanoid robot,” Autonomous robots, vol. 35, pp. 161–176, 2013.
- [20] B. Yao and M. Tomizuka, “Smooth robust adaptive sliding mode control of manipulators with guaranteed transient performance,” 1996.
- [21] Z. Gao, “Scaling and bandwidth-parameterization based controller tuning,” in Proceedings of the 2003 American Control Conference, 2003., vol. 6, 2003, pp. 4989–4996.
- [22] C. D. Bellicoso, C. Gehring, J. Hwangbo, P. Fankhauser, and M. Hutter, “Perception-less terrain adaptation through whole body control and hierarchical optimization,” in 2016 IEEE-RAS 16th International Conference on Humanoid Robots (Humanoids). IEEE, 2016, pp. 558–564.